

## Postcotunnite phase of the intermetallic compound AuIn<sub>2</sub> at high pressure

B. K. Godwal,<sup>1</sup> S. Speziale,<sup>2</sup> M. Voltolini,<sup>3</sup> R. Wenk,<sup>1</sup> and R. Jeanloz<sup>1,4</sup>

<sup>1</sup>*Department of Earth and Planetary Science, University of California, Berkeley, California 94720, USA*

<sup>2</sup>*Deutsches GeoForschungsZentrum, Section 3.3, Telegrafenberg, 9 24473 Potsdam, Germany*

<sup>3</sup>*Sincrotrone Trieste, SS14, Science Park, Basovizza, Trieste 34012, Italy*

<sup>4</sup>*Department of Astronomy, University of California, Berkeley, California 94720, USA*

(Received 15 February 2010; revised manuscript received 21 July 2010; published 24 August 2010)

We report a structural phase transition in AuIn<sub>2</sub> above 25 GPa. The inferred structure of this phase is post cotunnite (*P112<sub>1</sub>/a*). Combining the new results with previously observed behavior of AuIn<sub>2</sub>, we propose a sequence of structural transitions from CaF<sub>2</sub> (*Fm3m*) to amorphous phase at 24 GPa to monoclinic (*P112<sub>1</sub>/a*) structure at 25.6 GPa. During decompression the high-pressure phase is preserved to the pressure of 9.4 GPa and it finally transforms back to the *Fm3m* phase. Analysis of volume reduction and bulk modulus increase reveals close similarity with the postcotunnite phase observed in PbCl<sub>2</sub>. This study is important in understanding the behavior of metallic phases of various oxides of geophysical interest which exist in CaF<sub>2</sub> fluorite-type structure.

DOI: [10.1103/PhysRevB.82.064112](https://doi.org/10.1103/PhysRevB.82.064112)

PACS number(s): 61.50.Ks, 71.10.Hf, 64.30.-t, 71.20.-b

Prediction of phase transitions in materials, resolving controversies among measurements and unraveling the underlying transformation mechanisms provide important motivations for condensed matter theory.<sup>1-3</sup> High-pressure experiments have thus stimulated much theoretical work and prompted significant improvements in density-functional theories for exchange and correlation potentials beyond the local-density approximation.<sup>4,5</sup>

AX<sub>2</sub> (A=Au, X=In, Ga, Al) intermetallic compounds have attracted considerable attention in the recent past,<sup>6-11</sup> an example being high-resolution x-ray diffraction measurements indicating that AuIn<sub>2</sub> undergoes an isostructural electronic phase transition near 3 GPa and amorphizes at 24 GPa.<sup>12</sup> Being initially in the *Fm3m* fluorite (CaF<sub>2</sub>) structure, AuIn<sub>2</sub> is a potential high-pressure analog for SiO<sub>2</sub>, an oxide of interest for planetary geophysics.

The present study is intended to search for new crystalline phases of AuIn<sub>2</sub>, above the amorphization pressure, motivated by past reports of pressure-induced phase transitions in CaF<sub>2</sub>.<sup>13-23</sup> These studies show that CaF<sub>2</sub> transforms from the face-centered cubic fluorite structure (*Fm3m*) to an orthorhombic PbCl<sub>2</sub>-type (*Pnma*) structure at pressures between 8 and 10 GPa. Some electronic-structure calculations indicate that the band gap of CaF<sub>2</sub> increases with pressure,<sup>20-22</sup> becoming a direct gap due to the *Fm3m* to *Pnma* transition and then showing signatures of band-overlap metallization near 210 GPa.<sup>20</sup> However, Wu *et al.*'s<sup>22</sup> electronic-structure calculations using full-potential linearized augmented plane waves with combination of local orbitals do not indicate band closure up to 218 GPa. Based on their total-energy calculations for various structures, they predict a sequence of structural phase transitions from CaF<sub>2</sub> (*Fm3m*), to PbCl<sub>2</sub> (*Pnma*) to Ni<sub>2</sub>In (*P6<sub>3</sub>/mmc*).

Band gaps are not reliably estimated using density functional theory but the prediction of structural phase transitions based on total-energy calculations is expected to be less subject to systematic error. The *Fm3m* to *Pnma* structural phase transition has already been observed experimentally,<sup>14,19</sup> for example, but the transition to *P6<sub>3</sub>/mmc* has not yet been detected for CaF<sub>2</sub>. Although CaF<sub>2</sub> is ionic at ambient condi-

tions, it is important to look for the Ni<sub>2</sub>In phase in the context of understanding its possible metallization at high pressures; AuIn<sub>2</sub> thus serves as a relevant analog compound for experimental study.

Sample preparation and initial characterization have been described previously.<sup>12</sup> Briefly, single-phase AuIn<sub>2</sub> (*Fm3m* structure with lattice parameter  $a=6.5170$  ( $\pm 0.0007$ ) Å) was ground to 5–10 μm average grain size, and loaded into a ~120 μm diameter sample chamber drilled out of a 250-μm thick stainless-steel foil that had been indented to a final thickness of ~45 μm. The sample was compressed between two diamond anvils with 230-μm culets, using a mixture of methanol-ethanol-water (16:3:1 volume ratio) as pressure-transmitting medium. A 10 μm-size fragment of Au foil and a few specks of ruby were loaded as pressure calibrants. High-pressure experiments were performed using a short piston-cylinder diamond-anvil cell at beamline 12.2.2 of the Advanced Light Source at Lawrence Berkeley National Laboratory.<sup>21</sup> X-ray powder diffraction patterns were collected in angle-dispersive geometry, using monochromatic radiation of wavelength  $\lambda=0.48593$  ( $\pm 0.00004$ ) Å and a MAR345 image-plate detector placed at a distance of 380.116 ( $\pm 0.001$ ) mm from the sample. The x-ray beam width was approximately 100 μm in the horizontal and vertical directions.

All experiments were performed at room temperature, and pressure was determined both by the ruby fluorescence<sup>24</sup> and by x-ray diffraction of Au using the 300 K isotherms of Heinz and Jeanloz.<sup>25</sup> and Shim *et al.*<sup>26</sup> The sample-to-detector distance, image center and detector tilt were calibrated by collecting the diffraction pattern of powdered LaB<sub>6</sub> at ambient conditions. The software package FIT2D (Ref. 27) was used both for beam-position and sample-to-detector distance calibrations, and to integrate the two-dimensional diffraction images to obtain one-dimensional patterns.

Evolution of the x-ray diffraction patterns as a function of pressure shows that AuIn<sub>2</sub> undergoes a structural phase transition above 25.6 GPa (Fig. 1), and it is clear that the new phase is preserved to 9.4 GPa on decompressing at room temperature (Fig. 2). Finally, AuIn<sub>2</sub> transforms back to the

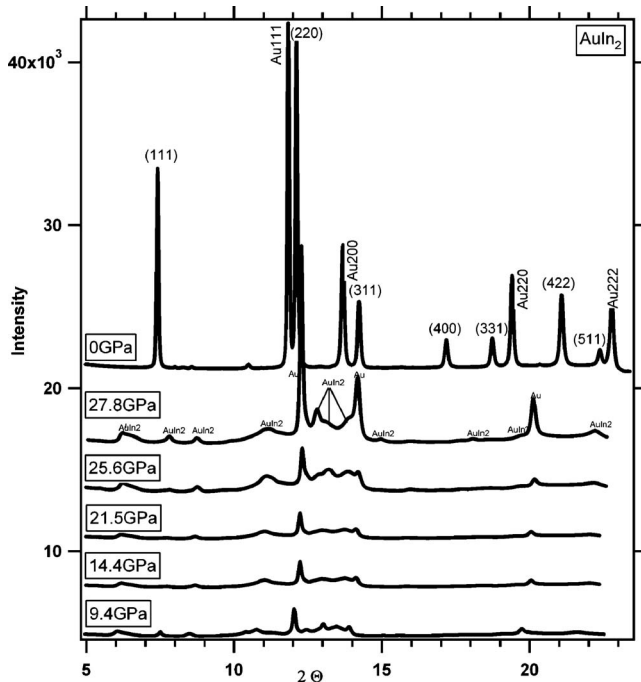


FIG. 1. X-ray diffraction patterns of  $\text{AuIn}_2$  as a function of pressure at room temperature. Patterns at 27.8 and 25.6 GPa were collected on compression, and all the others on decompression (refer to Fig. 3 for indexing of the transformed patterns).

ambient  $Fm\bar{3}m$  phase, with the starting value of lattice parameter, when pressure is fully released. For comparison, a previous study<sup>6</sup> identified a structural phase transition near 9 GPa on compression, the difference with the present study (and Ref. 12) being potentially attributable to differences in stress environments within the diamond-anvil cell.<sup>28</sup>

We employed the software package EXPO (Ref. 29) to index the observed powder-diffraction patterns in order to determine the structure and consistent unit-cell parameters for the high-pressure phase. The program indexed the pattern in possible orthorhombic and monoclinic cells but failed to uniquely determine the structure due to deterioration in the quality of data at high pressure. Specifically, the coarse-grained sample produced variable peak intensities, affecting the structure determination; however, lattice parameters could still be reliably estimated.

In order to obtain lattice parameters, we analyzed the x-ray diffraction spectra by the Le Bail whole-pattern fitting method. This approach is independent of the unit-cell content but effective for refining lattice parameters, especially if compared with techniques fitting the positions of only a few peaks. In the present analysis, we therefore considered structures that had been experimentally observed or theoretically predicted in similar systems. We confirmed through Le Bail refinement using general structure analysis system (GSAS) (Ref. 30) that neither  $\text{PbCl}_2$  ( $Pnma$ ) nor  $\text{Ni}_2\text{In}$  ( $P6_3/mmc$ ) structures can fit the high-pressure  $\text{AuIn}_2$  data, hence rule both of them out as possible candidates for the new high-pressure phase.

Refinements with the monoclinic structure ( $P112_1/a, Z=8$ ) were also considered because  $\text{BaX}_2$  compounds (with  $X=\text{Cl, Br, I}$ ), which are stable at ambient conditions in the

cotunnite structure ( $Pnam, Z=4$ )—the same structure as one of the high-pressure phases of  $\text{SiO}_2$ —transform to  $P112_1/a$  structure between 5 and 15 GPa at room temperature.<sup>31–33</sup> Leger and co-workers observed that across the structural transition the low-pressure cotunnite cell of  $\text{BaCl}_2$ ,  $\text{BaBr}_2$ , and  $\text{BaI}_2$  doubles along  $a$ , with orthogonal distortion to  $87^\circ$ – $89^\circ$ . They also observed an increase in the coordination number of Ba from 9 to 10.<sup>29–31</sup> The high-pressure monoclinic structure is a distortion of the  $\text{Co}_2\text{Si}$  ( $Pnam, Z=4$ ) type found by the same authors in intermetallic  $AB_2$  compounds (with  $A=\text{Pb, Sn}$  and  $B=\text{Cl}$ ).<sup>33</sup>

Using the cell parameters obtained from EXPO, we find good agreement of the data with the diffraction patterns refined for the monoclinic structure ( $P112_1/a, Z=8$ ) at 27.8 GPa on compression, and at 19 and 9.4 GPa on decompression (Table I, Fig. 2). The  $a$  and  $b$  cell parameters of the monoclinic phase are approximately related to the low-pressure cubic cell by  $a_{mc}=2^*a_c$  and  $b_{mc}=a_c^*/\sqrt{2}$ , and  $c_{mc}$  is about 5% less than  $a_c/(\sqrt{2})$  (subscripts  $mc$  and  $c$  refer to monoclinic and cubic structures, respectively).

In order to have the confidence in the use of existing structure available in the literature for the high pressure analysis of data we attempted Rietveld refinement using material analysis using diffraction (MAUD) (Ref. 34) and GSAS (Ref. 30) for the measurement carried out at 9.4 GPa. We found that most of the prominent peaks in the diffraction profile could be accounted for by a change of the atomic positions with respect to those listed by Leger *et al.*<sup>32</sup> for  $\text{PbCl}_2$ . We noticed no difference in the refined pattern with and without texture using MAUD. Although there were differences in the refined positions of atoms using MAUD and GSAS the lattice parameters were in agreement with each other (lattice parameters within 1% and  $\gamma$  angle within 2%) and in reasonable agreement with values determined using Le Bail whole profile fit (lattice parameters within 2.5% and  $\gamma$  angle within 5% with agreement in volume less than 1%). We thus believe that lattice parameters from Le Bail fit are reliably determined.

We also analyzed the data collected for  $\text{AuIn}_2$  using argon as pressure medium with a symmetric diamond anvil cell with limited opening which allowed diffraction data to the maximum  $2\theta$  of  $16^\circ$ , the details of which are discussed in the previous paper.<sup>12</sup> We found peak broadening and deterioration in the quality of data at high pressure. Thus use of another pressure transmitting medium also does not help in reducing the peak broadening. In view of such limitations we continued with Le Bail whole profile refinement for the analysis of data. Determination of the structure of the high pressure phase is an open problem due to deterioration of the quality of data obtained from powdered samples and there is serious need for high quality single crystal data.

Having determined its crystal structure, it is possible to characterize the effect of pressure on the high-pressure phase of  $\text{AuIn}_2$  (Fig. 3, Table I). The  $\gamma$  angle changes from  $78^\circ$  to  $84^\circ$  between 9.4 and 28 GPa (observed here on decompression), as compared with the variation from  $87^\circ$  to  $89^\circ$  documented by Leger *et al.*<sup>33</sup> for Ba halides between 5 and 15 GPa. This difference may be due to the fact that the monoclinic phase they observed forms from orthorhombic cotunnite whereas the high-pressure monoclinic structure of  $\text{AuIn}_2$

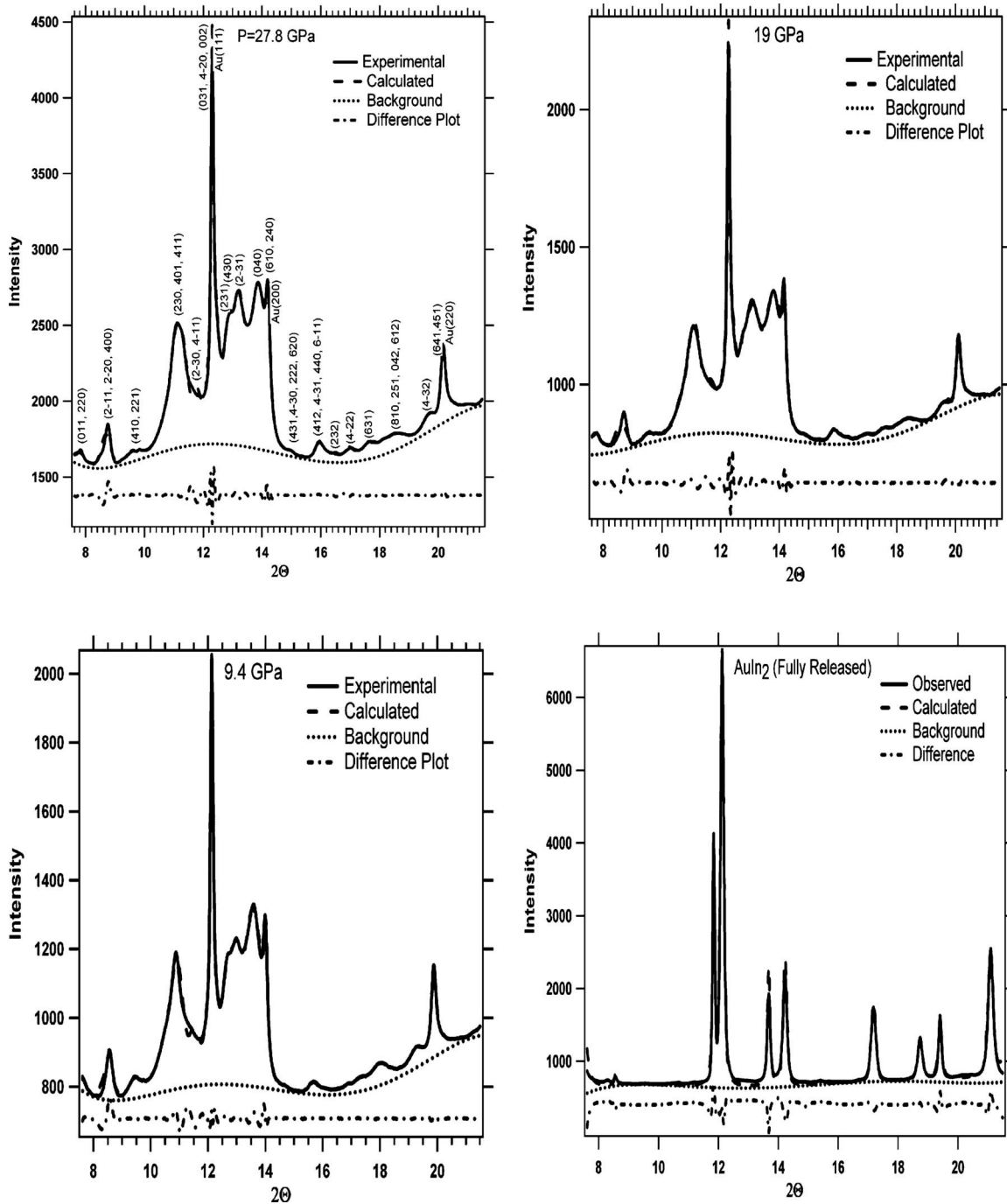


FIG. 2. Le Bail refined x-ray diffraction patterns for AuIn<sub>2</sub>: that at 27.8 GPa was collected on compression and the others on decompression. The indexing remains the same for patterns collected at 19 and 9.4 GPa, and the fully released pattern is the top one in Fig. 1.

forms from cubic *Fm3m* via an amorphous phase.<sup>12</sup> The axial ratios for BaX<sub>2</sub> halides in the postcotunnite phase are close to  $a/b=1.4$  and  $a/(b+c)=4.5$ , and our values for the monoclinic phase of AuIn<sub>2</sub> are 1.4 and 4.3.

We analyze the pressure-volume data (Fig. 4) using the Eulerian finite-strain formulation (see Ref. 35 and references therein). The low-pressure phase of AuIn<sub>2</sub> is subject to an electronic topological transition accompanied by an anomalous change in the pressure dependence of the bulk modulus between 2 and 3 GPa.<sup>12</sup> Therefore, we fit the lowest-pressure data only to 2.7 GPa, using the ambient pressure volume of

$276.79(\pm 0.096) \text{ \AA}^3$  and a third-order (Birch-Murnaghan) equation of state to obtain values of the bulk modulus and pressure derivative  $K_{T0}=56(\pm 2) \text{ GPa}$  and  $(\partial K_T/\partial P)_{T0}=18(\pm 4)$  (subscripts *T* and 0 indicate isothermal conditions and ambient pressure, respectively).

In order to determine the equation of state of the cubic phase between 2.7 and 18 GPa and the high-pressure monoclinic phase at higher pressures, we use an approach applicable when the zero-pressure volume is not known.<sup>35</sup> The equation of state is described in terms of a normalized pressure  $G=P/[3(1+2g)^{5/2}]$  as a function of Eulerian strain rela-

TABLE I. Unit-cell parameters of AuIn<sub>2</sub> postcotunnite high-pressure phase (space group *P112<sub>1</sub>/a*, *Z*=8)

Pressure (GPa)	<i>a</i> (Å)	<i>b</i> (Å)	<i>c</i> (Å)	$\gamma$ (deg)
27.8(±1.3)	12.145(5)	8.114(3)	4.510(1)	84.0(5)
19.0(±1.0)	12.298(2)	8.232(2)	4.531(2)	82.0(3)
9.40(±0.3)	12.599(2)	8.398(2)	4.602(2)	78.0(2)

tive to a reference volume  $V^*$ ,  $g=1/2[(V^*/V)^{2/3}-1]$ , such that the third-order Birch-Murnaghan equation of state corresponds to a second-order polynomial of  $G$  in  $g$ . A fit to the data for the cubic phase between 2.7 and 18 GPa yields  $V_0=278(\pm 2) \text{ \AA}^3$ ,  $K_{T0}=55(\pm 6) \text{ GPa}$ , and  $(\partial K_T/\partial P)_{T0}=10(\pm 1)$ , in agreement (within mutual uncertainties) with the parameters obtained below 2.7 GPa.

The unit-cell volume of the *P112<sub>1</sub>/a* phase was measured over a limited range of pressures ( $25.9 \pm 1$  to  $27.8 \pm 1$  GPa) and Eulerian strain ( $0.0808 \pm 0.0005$  to  $0.0819 \pm 0.0005$ ) under compression, so we also consider the data collected on decompression to 9.4 GPa (overall strain range of  $0.0283 \pm 0.0006$ ). Still, this range of strain is insufficient to reliably constrain a third-order equation of state,<sup>35</sup> so we performed a fit (Fig. 5) to the second-order (Birch) equation of state (which assumes  $(\partial K_T/\partial P)_{T0}=4$ ) to obtain  $V_0=249(\pm 2) \text{ \AA}^3$  and  $K_{T0}=168(\pm 13) \text{ GPa}$ . This corresponds to a threefold increase in the bulk modulus, relative to the low-pressure phase, similar to the findings of Leger *et al.*<sup>32</sup> for PbCl<sub>2</sub> and SnCl<sub>2</sub>.

In order to draw the similarity between the present high-pressure phase and the known postcotunnite phases of PbCl<sub>2</sub> and SnCl<sub>2</sub> compounds,<sup>32</sup> we compare the ratios of volumes and bulk moduli of high-pressure phase (phase II) to low-pressure phase (phase I) across the transition-pressure range from fluorite to postcotunnite structures of AuIn<sub>2</sub> and cotunnite to postcotunnite structures of PbCl<sub>2</sub> and SnCl<sub>2</sub> (Figs. 6 and 7). Based on our fitted equations of states for AuIn<sub>2</sub> and the available data for PbCl<sub>2</sub> and SnCl<sub>2</sub>, we observe a volume

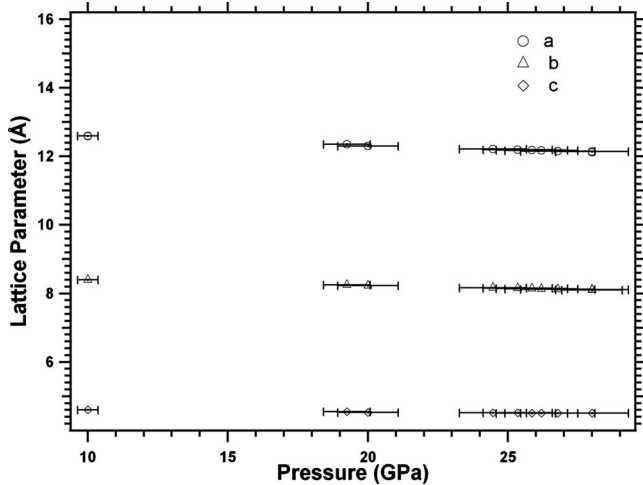


FIG. 3. Lattice parameters of the high-pressure monoclinic phase of AuIn<sub>2</sub> as a function of pressure.

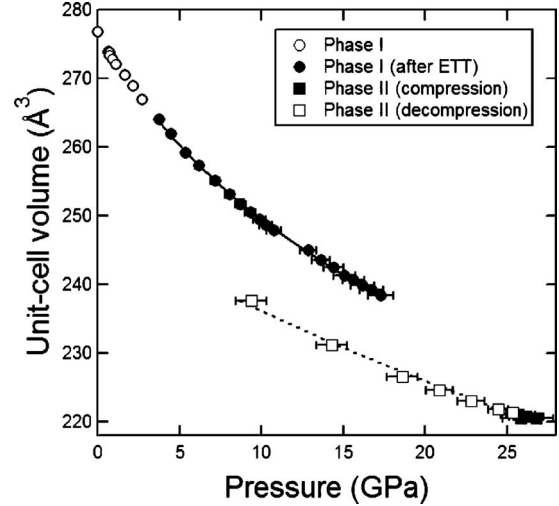


FIG. 4. Pressure-volume measurements for low- (cubic) and high-pressure (monoclinic) phases of AuIn<sub>2</sub> (I and II, respectively). Solid and dashed curves correspond to third- and second-order finite-strain equations of state, and the unit-cell volume of II is divided by 2 for comparison with I.

decrease and bulk modulus increase in agreement with that of PbCl<sub>2</sub> but not SnCl<sub>2</sub>.<sup>32</sup> However, from the comparison of the diffraction patterns for the postcotunnite structure of PbCl<sub>2</sub> (Fig. 4 in Ref. 32) and AuIn<sub>2</sub> depicted in Fig. 2 we note that the intensity ratios of the two patterns are different. This is due to large difference in the scattering factors of Pb and Cl compared with the smaller difference between Au and In. Particularly the ratio of the x-ray cross sections between Pb and Cl is almost an order of magnitude higher than that between Au and In in the energy range from 1 to 26 KeV.<sup>36</sup> We believe that this is the possible cause for the intensity difference between PbCl<sub>2</sub> and AuIn<sub>2</sub> although both belong to the same cotunnite phase.

In summary, we have observed the appearance of a high

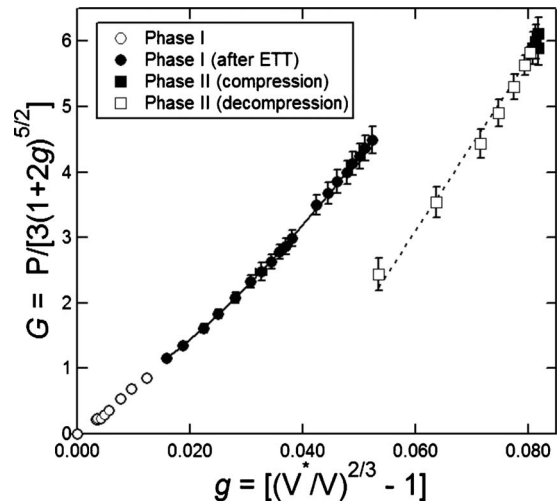


FIG. 5. Normalized pressure ( $G$ ) versus Eulerian strain ( $g$ ) for AuIn<sub>2</sub>. The strain is calculated with respect to the initial volume of phase I ( $V^*=276.79 \text{ \AA}^3$ ). Solid and dashed curves correspond to third- and second-order equations of state, respectively.

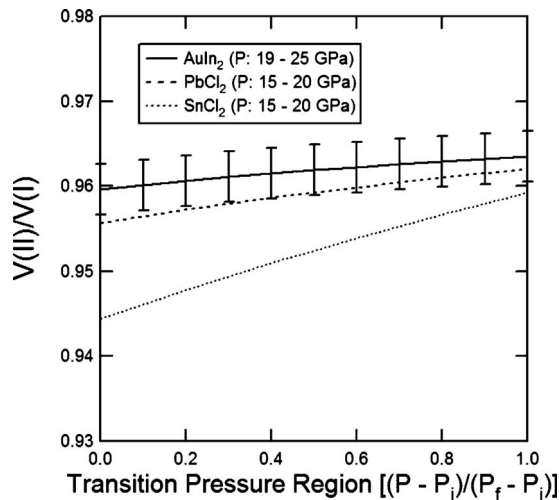


FIG. 6. Ratio  $V(II)/V(I)$  as a function of  $(P - P_i)/(P_f - P_i)$  at pressures ( $P$ ) in the range of the structural transition, where  $V(I)$  and  $V(II)$  correspond to volumes of the low- and high-pressure phases, respectively, and subscripts  $i$  and  $f$  are used for initial and final pressures defining the transition range.

pressure phase of  $\text{AuIn}_2$  with monoclinic ( $P112_1/a$ ) structure upon compression above 25.6 GPa at room temperature. The polymorph is retained to 9.4 GPa on decompression. The variation in axial parameters and the pressure-volume equation of state of the phase are similar to those of postcottonite phases of analog compounds. The present study points out the need for the improvement of the quality of the experimental data by using single crystal high pressure diffraction which may provide a testing ground for theoretical

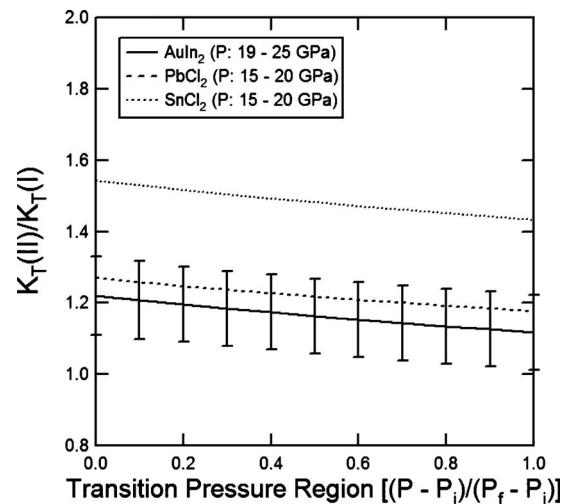


FIG. 7. Ratio  $[K_T(II)/K_T(I)]$  as a function of  $(P - P_i)/(P_f - P_i)$  at pressures ( $P$ ) in the range of structural transition, where  $K_T(I)$  and  $K_T(II)$  correspond to isothermal bulk moduli of the low- and high-pressure phases, respectively, and subscripts  $i$  and  $f$  are used for initial and final pressures defining the transition range.

modeling of high-pressure phases in  $\text{AuIn}_2$  and related compounds.<sup>37,38</sup>

We thank Simon Clark, Martin Kunz, and Sander Caldwell as well as the ALS staff for support on beamline 12.2.2. This work was supported by DOE, NSF, Lawrence Livermore National Laboratory, and the University of California.

<sup>1</sup>P. Hohenberg and W. Kohn, *Phys. Rev.* **136**, B864 (1964).

<sup>2</sup>W. Kohn and L. J. Sham, *Phys. Rev.* **140**, A1133 (1965).

<sup>3</sup>J. P. Perdew, K. Burke and M. Ernzerhof, *Phys. Rev. Lett.* **77**, 3865 (1996).

<sup>4</sup>G. A. Samara, *Physica B+C* **139-140**, 3 (1986).

<sup>5</sup>M. I. McMahon and R. J. Nelmes, *Chem. Soc. Rev.* **35**, 943 (2006).

<sup>6</sup>B. K. Godwal, S. Meenakshi, P. Modak, R. S. Rao, S. K. Sikka, V. Vijayakumar, E. Bussetto, and A. Lausi, *Phys. Rev. B* **65**, 140101(R) (2002).

<sup>7</sup>A. B. Garg, A. K. Verma, V. Vijayakumar, R. S. Rao, and B. K. Godwal, *Phys. Rev. B* **72**, 024112 (2005).

<sup>8</sup>A. B. Garg, B. K. Godwal, S. Meenakshi, P. Modak, R. S. Rao, S. K. Sikka, V. Vijayakumar, A. Lausi, and E. Bussetto, *J. Phys.: Condens. Matter* **14**, 10605 (2002).

<sup>9</sup>A. K. Verma, P. Modak, and S. M. Sharma, *J. Phys.: Condens. Matter* **20**, 325215 (2008).

<sup>10</sup>Q. Li, Y. Li, T. Cui, Y. Wang, L. J. Zhang, Y. Xie, Y. L. Niu, Y. M. Ma, and G. T. Zou, *J. Phys.: Condens. Matter* **19**, 425224 (2007).

<sup>11</sup>G. Ugur and F. Soybalp, *J. Phys.: Condens. Matter* **18**, 6777 (2006).

<sup>12</sup>B. K. Godwal, S. Speziale, S. M. Clark, J. Yan, and R. Jeanloz, *Phys. Rev. B* **78**, 094107 (2008).

<sup>13</sup>K. F. Seifert, *Ber. Bunsenges. Phys. Chem.* **70**, 1041 (1966).

<sup>14</sup>D. P. Dandekar and J. C. Jamieson, Proceedings of the Symposium on Crystal Structure at High Pressure, Seattle, WA, 1969, pp. 19-28/162.

<sup>15</sup>L. Gerward, J. S. Olsen, S. Steenstrup, S. Åsbrink, and A. Waskowska, *J. Appl. Crystallogr.* **25**, 578 (1992).

<sup>16</sup>A. M. Pendas, J. M. Recio, M. Florez, V. Luana, and M. Bermejo, *Phys. Rev. B* **49**, 5858 (1994).

<sup>17</sup>J. H. Burnett, Z. H. Levine, and E. L. Shirley, *Phys. Rev. B* **64**, 241102(R) (2001).

<sup>18</sup>S. Speziale and T. S. Duffy, *Phys. Chem. Miner.* **29**, 465 (2002).

<sup>19</sup>F. S. El'kin, O. B. Tsiok, L. G. Khvostantsev, and V. V. Brazhkin, *J. Exp. Theor. Phys.* **100**, 971 (2005).

<sup>20</sup>V. Kanchana, G. Vaitheeswaran, and M. Rjagopalan, *Physica B* **328**, 283 (2003).

<sup>21</sup>R. Khenata, B. Daoudi, M. Sahnoun, H. Baltache, M. Rerat, A. H. Reshak, B. Bouhaf, H. Abid, and M. Driz, *Eur. Phys. J. B* **47**, 63 (2005).

<sup>22</sup>X. Wu, S. Qin, and Z. Wu, *Phys. Rev. B* **73**, 134103 (2006).

<sup>23</sup>M. Kunz, A. A. MacDowell, W. A. Caldwell, D. Cambie, R. S. Celestre, E. E. Domning, R. M. Duarte, A. E. Gleason, J. M. Glossinger, N. Kelez, D. W. Plate, T. Yu, J. M. Zaug, H. A. Padmore, R. Jeanloz, A. P. Alivisatos, and S. M. Clark, *J. Synchrotron Radiat.* **12**, 650 (2005).

- <sup>24</sup>H. K. Mao, J. Xu, and P. M. Bell, *J. Geophys. Res.* **91**, 4673 (1986).
- <sup>25</sup>D. L. Heinz and R. Jeanloz, *J. Appl. Phys.* **55**, 885 (1984).
- <sup>26</sup>S. H. Shim, T. S. Duffy, and K. Takemura, *Earth Planet. Sci. Lett.* **203**, 729 (2002).
- <sup>27</sup>A. P. Hammersley, S. O. Svensson, M. Hanfland, A. N. Fitch, and D. Hausermann, *High Press. Res.* **14**, 235 (1996).
- <sup>28</sup>A. K. Verma, P. Modak, R. S. Rao, B. K. Godwal, and R. Jeanloz, *Phys. Rev. B* **75**, 014109 (2007).
- <sup>29</sup>A. Altomare, M. C. Burla, M. Camalli, B. Carrozzini, G. L. Cascarano, C. Giacovazzo, A. Guagliardi, A. G. G. Moliterni, G. Polidori, and R. Rizzi, *J. Appl. Crystallogr.* **32**, 339 (1999).
- <sup>30</sup>A. C. Larson and R. B. Von Dreele, Los Alamos National Laboratory Report No. LAUR 86-748, 2004 (unpublished).
- <sup>31</sup>J. M. Leger and A. Atouf, *J. Phys.: Condens. Matter* **4**, 357 (1992).
- <sup>32</sup>J. M. Léger, J. Haines, and A. Atouf, *Phys. Rev. B* **51**, 3902 (1995).
- <sup>33</sup>J. M. Léger, J. Haines, and A. Atouf, *J. Appl. Crystallogr.* **28**, 416 (1995).
- <sup>34</sup>L. Lutterotti, S. Matthies, H.-R. Wenk, A. J. Schultz, and J. W. Richardson, *J. Appl. Phys.* **81**, 594 (1997).
- <sup>35</sup>R. Jeanloz, *Geophys. Res. Lett.* **8**, 1219 (1981).
- <sup>36</sup>W. H. McMaster, N. Kerr Del Grande, J. H. Mallertt, and J. H. Hubbell, Lawrence Livermore National Laboratory Report No. UCRL-50174, 1969 (unpublished).
- <sup>37</sup>R. Martonák, A. R. Oganov, and C. W. Glass, *Phase Transitions* **80**, 277 (2007).
- <sup>38</sup>Y. Ma, A. R. Oganov, and Y. Xie, *Phys. Rev. B* **78**, 014102 (2008).